The Astrophysical Journal, 667: L53–L56, 2007 September 20


# VELOCITY DISPERSION PROFILES OF SEVEN DWARF SPHEROIDAL GALAXIES[1]

Matthew G. Walker,[2] Mario Mateo,[2] Edward W. Olszewski,[3] Oleg Y. Gnedin,[2] Xiao Wang,[4]
Bodhisattva Sen,[5] and Michael Woodroofe[5]

*Received 2007 March 12; accepted 2007 July 31; published 2007 September 10*

## ABSTRACT

We present stellar velocity dispersion profiles for seven Milky Way dwarf spheroidal (dSph) satellite galaxies. We have measured 8394 line-of-sight velocities ($\pm 2.5$ km s$^{-1}$) for 6804 stars from high-resolution spectra obtained at the Magellan and MMT telescopes. We combine these new data with previously published velocities to obtain the largest available kinematic samples, which include more than 5500 dSph members. All the measured dSphs have stellar velocity dispersion of order 10 km s$^{-1}$ that remains approximately constant with distance from the dSph center, out to and in some cases beyond the radius at which the mean surface brightness falls to the background level. Assuming dSphs reside within dark matter halos characterized by the NFW density profile, we obtain reasonable fits to the empirical velocity dispersion profiles. These fits imply that, among the seven dSphs, $M_{\rm vir} \sim 10^8$–$10^9\ M_\odot$. The mass enclosed at a radius of 600 pc, the region common to all data sets, lies in the range (2–7) $\times\ 10^7\ M_\odot$.

*Subject headings:* dark matter — galaxies: dwarf — galaxies: kinematics and dynamics — Local Group — techniques: radial velocities

## 1. INTRODUCTION

Spanning the absolute magnitude range $-13 \leq M_V \leq -4$ (Mateo 1998; Belokurov et al. 2007), dwarf spheroidal (dSph) galaxies represent the extreme end of the galaxy luminosity function. The Milky Way's (MW's) ~15 known dSph satellites have managed thus far to avoid and/or to survive interactions that consumed many of their siblings during hierarchical formation of the MW halo. Recent velocity measurements for several hundred stars per dSph (Kleyna et al. 2002, 2003, 2004; Muñoz et al. 2005, 2006; Walker et al. 2006a, 2006b; Simon & Geha 2007) demonstrate that dSph velocity dispersions remain approximately flat with radius. Analyses that recover $M(r)$ from the Jeans equation conclude that dSphs possess extended and dominant DM halos (e.g., Łokas 2002), unless stellar velocity distributions are highly anisotropic or ongoing tidal disruption invalidates the assumption of equilibrium (e.g., Kroupa 1997).

In this Letter we present velocity dispersion profiles for seven dwarf satellites of the Milky Way—Carina, Draco, Fornax, Leo I, Leo II, Sculptor, and Sextans. Profiles are calculated from new velocity data we have obtained using the Magellan and MMT telescopes (Walker et al. 2007; Mateo et al. 2007). After combining with previously published data, samples range in size from ~200 (Leo II) to ~2000 (Fornax) member stars per dSph, for a total of 5544 probable members in the seven dSphs. The new samples more than double the amount of existing dSph kinematic data and allow us to measure velocity dispersion profiles with unprecedented precision. All the measured dSphs exhibit approximately flat velocity dispersion profiles that can be fit reasonably well under the assumption that dSphs are equilibrium systems embedded within dark matter halos. We show that if the dark matter halos are characterized by the NFW density profile (Navarro et al. 1996) that results from *N*-body simulations of cold dark matter, the kinematic data suggest dSphs have $M_{\rm vir} \sim 10^8$–$10^9\ M_\odot$ and masses of (2–7) $\times\ 10^7\ M_\odot$ inside a radius of 600 pc.

## 2. OBSERVATIONS AND DATA

Over seven observing runs between 2004 March and 2007 January, we used the Michigan/MIKE Fiber System (MMFS) at the Magellan/Clay 6.5 m telescope to obtain 7383 high-resolution echelle spectra of 5793 individual red giant candidates in the dSph galaxies Carina, Fornax, Sculptor, and Sextans. Walker et al. (2007) describe the uniform data reduction procedure in detail. MMFS spectra sample the Mg-triplet (MgT) region, spanning 5140–5180 Å with effective resolution ~0.1 Å pixel$^{-1}$ ($R \sim 20{,}000$). We measure both stellar velocity and the pseudo–equivalent width of the magnesium absorption feature. The latter quantity correlates with surface gravity and helps determine dSph membership. Comparisons of repeat measurements for more than 1000 stars indicate median measurement errors of ~2.0 km s$^{-1}$ and ~0.06 Å, respectively.

In addition, we obtained 1183 spectra from 1011 red giant candidates in the dSphs Leo I, Leo II, and Draco using the multifiber Hectochelle spectrograph at the MMT 6.5 m telescope during three observing runs in March/April of 2005, 2006, and 2007 (see Mateo et al. 2007). Hectochelle spectra sample the MgT region over 5150–5300 Å with effective resolution 0.01 Å pixel$^{-1}$ ($R \sim 25{,}000$). Repeat measurements for more than 100 stars with Hectochelle indicate velocity errors of ~2.6 km s$^{-1}$.

To these new, homogeneous data sets we add 2239 velocities previously published for red giant candidates in the observed dSphs (Carina: Mateo et al. 1993; Muñoz et al. 2006; Draco: Armandroff et al. 1995; Kleyna et al. 2002; Fornax: Mateo et al. 1991; Walker et al. 2006a; Leo I: Mateo et al. 1998; Koch et al. 2007b; Leo II: Vogt et al. 1995; Koch et al. 2007a; Sculptor: Westfall et al. 2006; Sextans : Hargreaves et al. 1994; Kleyna et al. 2004). We correct for zero-point offsets and combine measurements of common stars using the weighted (by measurement errors) mean velocity. We do not correct for the slopes noted by Walker et al. (2007) when comparing MgT

[1] This paper includes data gathered with the 6.5 m Magellan Telescopes at Las Campanas Observatory, Chile, and with the 6.5 m MMT telescope.

[2] Department of Astronomy, University of Michigan, Ann Arbor, MI 48109.
[3] Steward Observatory, University of Arizona, Tucson, AZ 85721.
[4] Department of Mathematics and Statistics, University of Maryland, Baltimore County, Baltimore, MD 21250.
[5] Department of Statistics, University of Michigan, Ann Arbor, MI 48109.

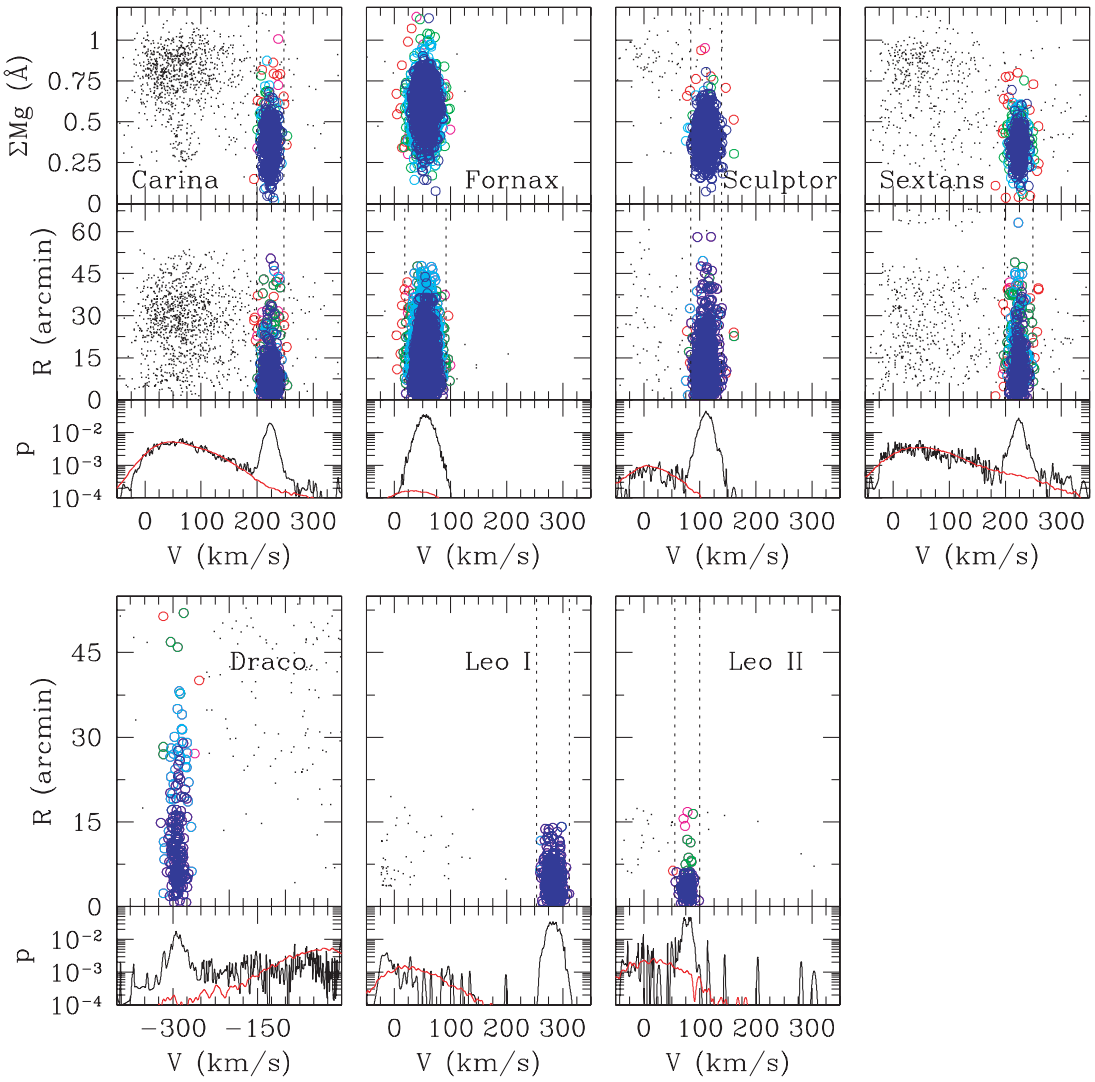


FIG. 1.—Mg pseudo–equivalent width, projected distance, and membership fraction vs. velocity for new dSph samples obtained with Magellan MMFS and MMT Hectochelle (Mg strength is unavailable for Hectochelle observations). Marker color indicates the probability that the star is a dSph member. Black, red, magenta, green, cyan, and blue markers signify $\hat{P}_{\rm dsph} < 0.01$ and $\hat{P}_{\rm dsph} > 0.01$, >0.50, >0.68, >0.95, and >0.99, respectively. Pairs of dotted lines enclose stars that would pass conventional membership tests based on a 3 $\sigma$ velocity threshold. Red lines in the bottom subpanels indicate the interloper distribution predicted by the Besançon Milky Way model.

velocities to those measured from the calcium triplet; doing so would have no significant impact on the velocity dispersion profiles because the relevant combined samples are dominated by MMFS data.

We evaluate the probability $P_{{\rm dsph}_i}$ that the $i$th star is a dSph member using up to three pieces of information—velocity $V_i$, magnesium strength $W_i$ (available only for MMFS samples), and position; a priori, stars projected farther from the dSph center are less likely to be members. We assume that (1) the joint distribution of $V$ and $W$ for the members of a given dSph is a bivariate Gaussian; (2) interlopers have magnesium strengths following a univariate Gaussian distribution; and (3) interlopers have a non-Gaussian velocity distribution that we estimate numerically from the Besançon Milky Way model (Robin et al. 2003). We use an iterative, expectation-maximization (EM) algorithm (Sen et al. 2007) to recover maximum-likelihood estimates of the Gaussian means and variances as well as the individual membership probabilities (see M. G. Walker et al. 2007, in preparation, for full details of the algorithm). Black markers in Figure 1 identify the most likely interlopers ($\hat{P}_{{\rm dsph}_i} < 0.01$), while colored markers signify larger $\hat{P}_{{\rm dsph}_i}$ (see caption to Fig. 1). In subsequent calculations we weigh each data point by $\hat{P}_{{\rm dsph}_i}$.

Middle subpanels in Figure 1 plot velocity against angular distance from the dSph center. Bottom subpanels indicate the overall velocity distribution; red lines give the expected distributions of interloper velocities, per the Besançon model. For dSphs observed with a high degree of contamination (Carina, Sextans), we find excellent agreement between the predicted and observed velocity distributions of foreground stars. Table 1 lists for each dSph the numbers of newly observed stars, total stars after combining with published data, and member stars $N_{\rm dsph} = \sum_{i=1}^{N_{\rm tot}} \hat{P}_{{\rm dsph}_i}$.

## 3. VELOCITY DISPERSION AND NFW PROFILES

We estimate line-of-sight velocity dispersion profiles after dividing each sample into $\sim(N_{\rm dsph})^{1/2}$ bins according to projected distance from the dSph center. For a given sample we define bins (circular annuli) such that all contain approximately

TABLE 1
SUMMARY OF dSph VELOCITY SAMPLES AND NFW PARAMETERS

| Galaxy | $N_{new}$ | $N_{tot}$ | $N_{dsph}$ | $\beta$ | $M_{vir}$ ($10^7\ M_\odot$) | $M_{r_{max}}$ ($10^7\ M_\odot$) | $M_{600}$ ($10^7\ M_\odot$) |
|---|---|---|---|---|---|---|---|
| Carina ..... | 1833 | 2567 | 899 | −0.5 | 20 | 3.5 | 2.0 |
| Draco ..... | 512 | 738 | 413 | −1 | 400 | 9.0 | 6.9 |
| Fornax ..... | 1924 | 2085 | 2008 | −0.5 | 100 | 18 | 4.6 |
| Leo I ..... | 371 | 483 | 416 | −0.5 | 100 | 7.3 | 4.5 |
| Leo II ..... | 128 | 264 | 213 | 0 | 40 | 4.3 | 2.8 |
| Sculptor ..... | 1089 | 1214 | 1091 | −0.5 | 100 | 8.2 | 4.3 |
| Sextans ..... | 947 | 1032 | 504 | −2 | 30 | 5.4 | 2.5 |

equal numbers of dSph members. Thus the number of stars, including interlopers, in each bin may vary, but for all bins, $\Sigma_{i=1}^{N_{bin}} \hat{P}_{dsph_i} \sim (N_{dsph})^{1/2}$. We use a Gaussian maximum-likelihood method (see Walker et al. 2006a) to estimate the velocity dispersion within each bin.

Left-hand panels Figure 2 display the resulting velocity dispersion profiles, which generally are flat. The outer profile of Draco shows no evidence for a rapidly falling dispersion, contrary to evidence presented by Wilkinson et al. (2004) but consistent with the result of Muñoz et al. (2005).[6] In fact the outer profiles of Draco, Carina, and perhaps Sculptor show gently rising dispersions. While it is likely that at least in Carina this behavior is associated with the onset of tidal effects (Muñoz et al. 2006), McConnachie et al. (2007) point out that the tendency of some dSphs to have systematically smaller velocity dispersions near their centers is perhaps the result of distinct and poorly mixed stellar populations (Tolstoy et al. 2004; Battaglia et al. 2006; Ibata et al. 2006). Either explanation complicates a thorough kinematic analysis; in the present, simplified analysis we assume all stars belong to a single population in virial equilibrium.

Dashed lines in Figure 2 are velocity dispersion profiles calculated for single-component King models (King 1962) conventionally used to characterize dSph surface brightness profiles. The adopted King models are those fit by Irwin & Hatzidimitriou (1995, hereafter IH95) and normalized to match the

[6] We have not included the unpublished data of Wilkinson et al. (2004) or Muñoz et al. (2005) in our calculations of the velocity dispersion profiles of Draco.

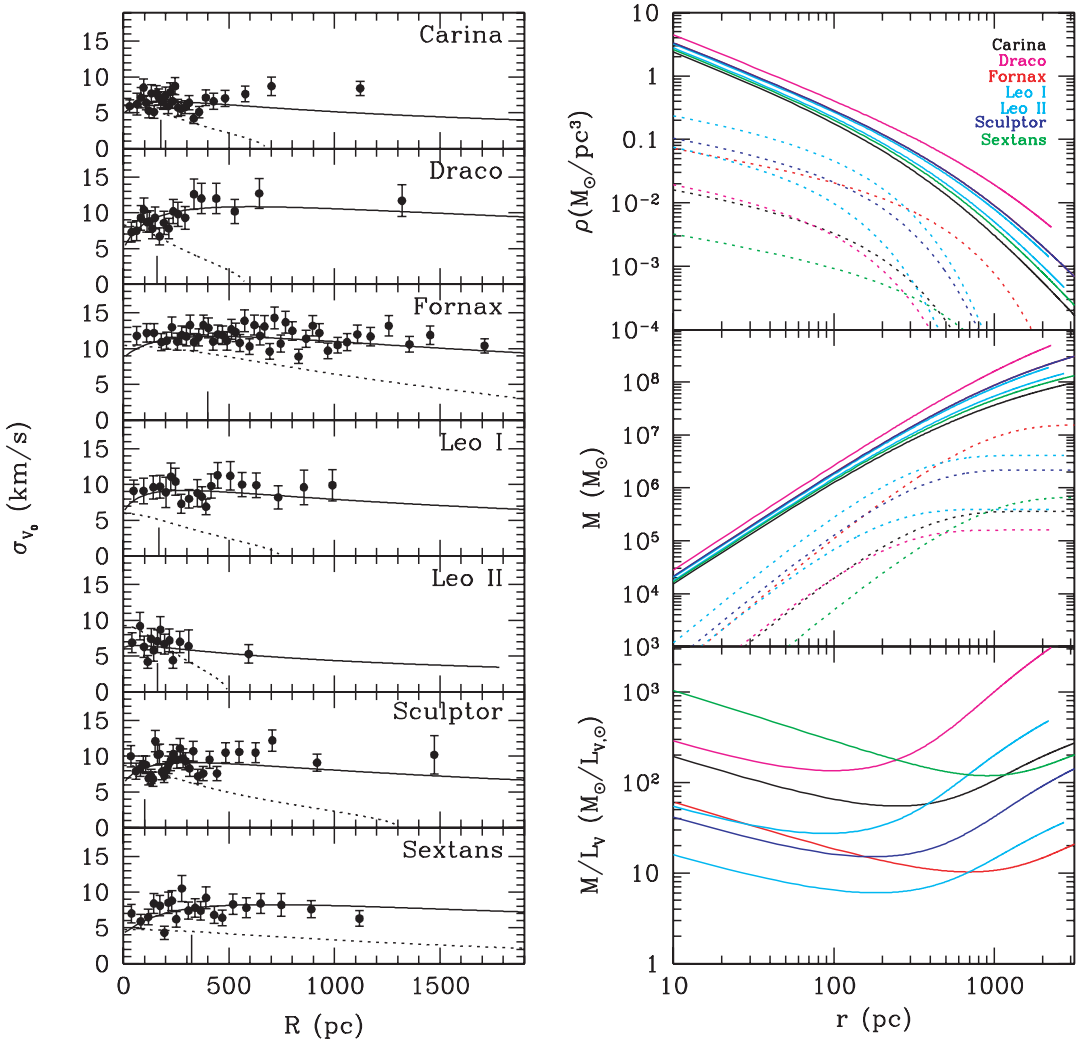


FIG. 2.—*Left*: Projected velocity dispersion profiles for seven Milky Way dSph satellites. Overplotted are profiles corresponding to mass-follows-light (King 1962) models (*dashed lines*; these fall to zero at the nominal "edge" of stellar distribution), and best-fitting NFW profiles that assume $\beta$ = constant. Short, vertical lines indicate luminous core radii (IH95). Distance moduli are adopted from Mateo (1998). *Right*: Solid lines represent density, mass, and *M*/*L* profiles corresponding to best-fitting NFW profiles. Dotted lines in the top and middle panels are baryonic density and mass profiles, respectively, following from the assumption that the stellar component (assumed to have $M/L = 1$) has exponentially falling density with scale length given by IH95.

central velocity dispersion. Their systematic failure to predict flat profiles removes any doubt that (Newtonian) mass-follows-light, equilibrium models provide a poor description of dSph kinematics.

In forthcoming papers we examine evidence for tidal effects and explore the range of dark matter density profiles that are consistent with the dSph velocity data. Here we simply show that dark matter halos having the NFW density profile can fit the data reasonably well. Under the assumptions of (1) spherical symmetry, (2) dynamic equilibrium, (3) radially constant velocity anisotropy $\beta \equiv 1 - \sigma_\theta^2/\sigma_r^2$, and (4) that dSph surface brightness declines exponentially with radius, with central value and scale length adopted from IH95, we use the Jeans equation (e.g., eq. [A15] of Mamon & Łokas 2005) to calculate projected velocity dispersion profiles expected for NFW halos over a range of plausible virial masses. Assuming the relationship between $M_{\rm vir}$ and halo concentration found by Jing (2000, see also Mamon & Łokas 2005; Koch et al. 2007b), we fit to the empirical velocity dispersion profiles using just two free parameters, $M_{\rm vir}$ and $\beta$. Solid lines in the left-hand panels of Figure 2 indicate the best-fitting NFW models, and Table 1 lists the associated parameters, including $M_{r_{\rm max}}$, the enclosed (dark plus luminous) mass at the outermost profile point. The right-hand panels of Figure 2 display mass-density, mass, and $M/L$ profiles corresponding to the best-fitting NFW models.

Strigari et al. (2007) show that dSph masses within $r \leq 600$ pc ($M_{600}$) are constrained robustly by kinematic data, irrespective of the assumed form of the density profile. This radius is convenient for practical reasons in our analysis as it covers the largest region common to all the data sets and is sufficiently small that one expects tidal effects inside this radius to be negligible (Read et al. 2006). Integrating the density profiles for the stellar (for which we assume $M/L = 1$) and dark components, we find that $M_{600}$ lies in the range $(2–7) \times 10^7\ M_\odot$ among the seven dSphs (Table 1). This narrow range is consistent with the notion that these dSphs, while exhibiting order-of-magnitude variability in luminosity, occupy dark halos of similar mass (Mateo et al. 1993).

We thank the staff at the Las Campanas and MMT Observatories. This work is supported by NSF grants AST 05-07453, AST 02-06081, AST 00-98518, AST 02-05790, and AST 05-07511.

REFERENCES

Armandroff, T. E., Olszewski, E. W., & Pryor, C. 1995, AJ, 110, 2131
Battaglia, G., et al. 2006, A&A, 459, 423
Belokurov, V., et al. 2007, ApJ, 654, 897
Hargreaves, J. C., Gilmore, G., Irwin, M. J., & Carter, D. 1994, MNRAS, 269, 957
Ibata, R., Chapman, S., Irwin, M., Lewis, G., & Martin, N. 2006, MNRAS, 373, L70
Irwin, M., & Hatzidimitriou, D. 1995, MNRAS, 277, 1354 (IH95)
Jing, Y. P. 2000, ApJ, 535, 30
King, I. 1962, AJ, 67, 471
Kleyna, J., Wilkinson, M. I., Evans, N. W., Gilmore, G., & Frayn, C. 2002, MNRAS, 330, 792
Kleyna, J. T., Wilkinson, M. I., Evans, N. W., & Gilmore, G. 2004, MNRAS, 354, L66
Kleyna, J. T., Wilkinson, M. I., Gilmore, G., & Evans, N. W. 2003, ApJ, 588, L21
Koch, A., Kleyna, J. T., Wilkinson, M. I., Grebel, E. K., Gilmore, G. F., Evans, N. W., Wyse, R. F. G., & Harbeck, D. R. 2007a, AJ, 134, 566
Koch, A., Wilkinson, M. I., Kleyna, J. T., Gilmore, G. F., Grebel, E. K., Mackey, A. D., Evans, N. W., & Wyse, R. F. G. 2007b, ApJ, 657, 241
Kroupa, P. 1997, NewA, 2, 139
Łokas, E. L. 2002, MNRAS, 333, 697
Mamon, G. A., & Łokas, E. L. 2005, MNRAS, 363, 705
Mateo, M., Olszewski, E., Welch, D. L., Fischer, P., & Kunkel, W. 1991, AJ, 102, 914
Mateo, M., Olszewski, E. W., Pryor, C., Welch, D. L., & Fischer, P. 1993, AJ, 105, 510
Mateo, M., Olszewski, E. W., Vogt, S. S., & Keane, M. J. 1998, AJ, 116, 2315
Mateo, M., Olszewski, E. W., & Walker, M. G. 2007, submitted to ApJ
Mateo, M. L. 1998, ARA&A, 36, 435
McConnachie, A. W., Peñarrubia, J., & Navarro, J. F. 2007, MNRAS, 380, L75
Muñoz et al. 2005, ApJ, 631, L137
———. 2006, ApJ, 649, 201
Navarro, J. F., Frenk, C. S., & White, S. D. M. 1996, ApJ, 462, 563
Read, J. I., Wilkinson, M. I., Evans, N. W., Gilmore, G., & Kleyna, J. T. 2006, MNRAS, 366, 429
Robin, A. C., Reylé, C., Derrière, S., & Picaud, S. 2003, A&A, 409, 523
Sen, B., Walker, M. G., & Woodroofe, M. 2007, Statistica Sinica, submitted
Simon, J. D., & Geha, M. 2007, ApJ, in press (arXiv:0706.0516)
Strigari, L. E., Bullock, J. S., Kaplinghat, M., Diemand, J., Kuhlen, M., & Madau, P. 2007, preprint (arXiv:0704.1817)
Tolstoy, E., et al. 2004, ApJ, 617, L119
Vogt, S. S., Mateo, M., Olszewski, E. W., & Keane, M. J. 1995, AJ, 109, 151
Walker, M. G., Mateo, M., Olszewski, E. W., Bernstein, R., Wang, X., & Woodroofe, M. 2006a, AJ, 131, 2114
Walker, M. G., Mateo, M., Olszewski, E. W., Bernstein, R. A., Sen, B., & Woodroofe, M. 2007, ApJS, 171, 389
Walker, M. G., Mateo, M., Olszewski, E. W., Pal, J. K., Sen, B., & Woodroofe, M. 2006b, ApJ, 642, L41
Westfall, K. B., Majewski, S. R., Ostheimer, J. C., Frinchaboy, P. M., Kunkel, W. E., Patterson, R. J., & Link, R. 2006, AJ, 131, 375
Wilkinson, M. I., Kleyna, J. T., Evans, N. W., Gilmore, G. F., Irwin, M. J., & Grebel, E. K. 2004, ApJ, 611, L21